ORTIONS
OF THIS
OCUMENT
ARE
LEGIBLE

LA-UR-82-834

Conf-820627--4

MASTER

LA-UR--82-834

DE82 012145

TITLE: AN EXPERIMENTAL AND THEORETICAL STUDY OF SALT-GRADIENT POND INTERFACE BEHAVIOR

AUTHOR(S): K. A. Meyer, D. P. Grimmer, G. F. Jones

SUBMITTED TO: To be published in the Proceedings of the 1982 Annual Meeting, American Section of the International Solar Energy Society

DISCLAIMER

DISTRIBUTION OF THIS DOCUMENT IS UNLIMITED

Los Alamos

Los Alamos National Laboratory
Los Alamos, New Mexico 87545

AN EXPERIMENTAL AND THEORETICAL STUDY OF SALT-GRADIENT POND INTERFACE BEHAVIOR*

by

K. A. Meyer, D. P. Grimmer, G. F. Jones
Los Alamos National Laboratory
Solar Energy Group, M.S. K571
Los Alamos, NM 87545

ABSTRACT

We describe an extension of our numerical model to include the effect of wind shear on upper convective region growth. We also report on laboratory experiments designed to investigate interface motion in salt-gradient ponds, and we present a comparison of our numerical model prediction with an experimental result.

We briefly review our numerical model treatment of the double diffusive effects at the interfaces between convecting and nonconvecting regions in solar ponds, and we describe an approach that incorporates wind-generated turbulent entrainment into the interface treatment. We find agreement of the calculated behavior with observations made on a solar pond.

Two kinds of interface experiments are discussed. The first kind consists of tank experiments designed to give information on interface motion, and on salt and heat transport across interfaces. Numerical model predictions are compared with experimental data. The second type of experiments combine flow-visualization techniques with temperature and salinity measurements. These experiments reveal the flow structure in the neighborhood of the interface.

1. INTRODUCTION

The behavior of interfaces separating convecting and nonconvecting regions in salt-gradient ponds is of great importance in determining pond performance. Growth of the upper and lower convecting regions results in the narrowing of the insulating, nonconvecting region, an increase in upward heat loss, and a reduction of the pond's efficiency. We are developing a numerical model to predict interface motion to facilitate pond design and operation.

The basic numerical model treating double diffusive interface transport has been described in detail in Ref. 1. In Section 2 we briefly review this basic model and then describe a treatment for including the interface motion induced by wind shear. The wind-shear treatment is formulated so that wind effects and the basic double diffusive effects are additive.

In Section 3 we describe our flow-visualization experiments that are designed to give an understanding of the basic flow patterns involved in interface salt transport and heat transport. The observations also allow us to evaluate models of interface transport proposed in the literature.

Section 4 describes an experiment in which we measure the salt flux, heat flux, and interface motion in laboratory solar pond simulation; our results are compared with those of other investigators. We also use the measured salt-to-heat flux ratio in a numerical model calculation of interface position, and compare this result with the experimental results.

2. NUMERICAL MODELING

2.1 Review of Basic Model

This model is described in detail in Ref. 1 and will be reviewed only briefly here.

The pond configuration assumed in the one dimensional numerical model is a three region system with boundary layers separating the convecting regions from the nonconvecting regions. The time dependent diffusion equation is used to determine

*This work was partially supported by the U.S. Department of Energy, Division of Solar Thermal Energy Systems.

both the heat flux and the salt flux. The temperature distribution in the pond is obtained from

$$\rho C_p \frac{\partial T}{\partial t} = \frac{\partial}{\partial x}\left(k_T \frac{\partial T}{\partial x}\right) + q(x,t) - L(x,t). \quad (1)$$

In the nonconvecting region, the molecular conductivity is used for k_T; in the convecting regions, an eddy conductivity is used.

The salinity profile is determined from

$$\frac{\partial \rho_s}{\partial t} = \frac{\partial}{\partial x}\left(D_s \frac{\partial \rho_s}{\partial x} + D_{ST} \frac{\partial T}{\partial t}\right). \quad (2)$$

The second term on the right is the Soret term; it represents salt transport induced by the temperature gradient. In the nonconvecting region, the molecular diffusivity is used for D_s, whereas an eddy diffusivity is used in the convecting region.

For an interface between convecting and nonconvecting regions to remain stationary, we must maintain static stability (density increasing downward)

$$\frac{\Delta \rho}{\Delta x} = \alpha \frac{\Delta T}{\Delta x} + \beta \frac{\Delta \rho_s}{\Delta x} \geq 0, \quad (3)$$

across the boundary layer separating these regions. If the condition of Eq. (3) is violated, the convecting region will encroach on the nonconvecting region.

The salt transport and heat transport across the interface boundary layers are obtained from empirical relations generated in various oceangraphic thermohaline studies (see, for example, Ref. 2). The boundary layer heat flux is a function of the temperature difference across the boundary layer and of the fluid properties. The salt flux is related to the heat flux by

$$\frac{\rho C_p \beta F_s}{\alpha H} = C. \quad (4)$$

We feel, at this time, that C is actually a function of the heat flux, H, and varies between 0.14 and 0.50.

In our numerical model, we have converted the empirical salt flux and heat flux to an effective boundary layer thermal conductivity, k_{T_A} and an effective salt diffusivity, D_s. The system of Eqs. (1-4) was replaced by its finite difference analog and solved using an implicit procedure.

2.2 Wind Induced Entrainment

The basic model described in the preceeding section accounts for both the interface salt flux and heat flux generated by local, thermally induced turbulence. In a solar pond we can expect to have added effects caused by externally induced turbulence generated either by wind action at the surface or by fluid injection or withdrawal in the convecting regions.

We are aware of only one reference, the work by Crapper (Ref. 3), dealing with the combined effects of double diffusive transport and externally generated turbulence. Although, his quantitative results cannot be generalized, his data indicates that external turbulence produces an increase in the interface salt flux and heat flux above those caused by thermal convection alone.

There is an extensive collection of work dealing with turbulent entrainment at a density interface between stably stratified fluids with only one diffusing quantity present. We are interested in the case of a wind-driven, uniform density convecting region that lies on a nonconvecting region, the latter having a stable density gradient. Under these conditions, we can correlate the entrainment of the gradient region with the wind shear and the Richardson number, Ri, by a relation of the form

$$\frac{u_e}{u_*} = C_1 \, Ri^{-n} , \quad (5)$$

where C_1 and n are empirical constants. The friction velocity, u_*, is related to the wind speed, w, by

$$u_* = \left(C_D \frac{\rho_a}{\rho}\right)^{1/2} w. \quad (6)$$

In order to combine the thermally induced double diffusive process with turbulent entrainment, we assume we can replace the entrainment velocity by appropriate "entrainment fluxes" resulting from mixing, and that these fluxes can be added to the double diffusive fluxes described in Section 2.1. Encroachment of the interface then results from the loss of static stability, Eq. (3), across the postulated interface boundary layer. This assumption of separate, additive contributions from both the double diffusive effect and the mechanical turbulence appears to be justified by our observations of relatively rare mixing events in double diffusive flow and similar observations by Turner (Ref. 4) for grid-generated turbulences.

The entrainment heat flux across the interface can be expressed as

$$H = u_e \rho C_p \Delta T, \quad (7)$$

whereas the salt flux is

$$F_S = -u_e \Delta \rho_S. \tag{8}$$

From these relations we define effective entrainment boundary-layer diffusivities, which are added to the double diffusive contributions.

2.3 Comparison With Experiment

We have used our wind-entrainment, double diffusive model to calculate the performance of the Miamisburg, Ohio, solar pond over a three-month period. Data for the pond performance were provided by L. Wittenberg and M. Harris of the Mound Facility, Miamisburg, Ohio.

It should be noted that during this period of operation, the salinity of the pond's lower convective layer was much lower than normal.

Initial temperature and salinity profiles were obtained from the data. Simple smooth fits were used for the insolation and ambient temperatures; an average wind speed of 4.0 m/s was used.

There is currently some uncertainity regarding the appropriate values for C_1 and n in Eq. (5). We tried two sets of values in our calculations. In the first case we used the values $C_1 = 0.075$, $n = 1$ as obtained by Wu (Ref. 5); whereas in the second case we used $C_1 = 1.5$, $n = 3/2$ as obtained by Kit, et al. (Ref. 6). Observed and calculated interface positions as a function of time are shown in Fig. 1. We see that the calculation with $n = 1$ gives good agreement with observations for both the upper and lower interfaces; the use of $n = 3/2$ underestimates the growth of the upper convective layer.

3. FLOW-VISUALIZATION EXPERIMENTS

Our flow-visualization experiments are directed both at obtaining an understanding of the flow patterns involved at a thermally driven, double diffusive interface and at assessing a simple mechanistic model of the interface proposed independently by Lindberg and Haberstroh (Ref. 7) and Linden and Shirtcliffe (Ref. 8).

The proposed model assumes the simultaneous growth of a thermal boundary layer and a salinity boundary layer from the diffusive core into the intermittant turbulent convection region. Because of the high thermal diffusivity, the thermal boundary layer outdistances the layer caused by salinity. Because the temperature distribution in the thermal layer is unstable, at some thickness the layer will break down and a bouyant element will be released. Such elements are described as thermal plumes. The thickness of the salinity boundary layer and the temperature boundary layer at breakdown can be calculated from stability considerations. If we assume that at breakdown both boundary layers are fully mixed into the convecting region, we can estimate the ratio of salt flux to heat flux caused by this mechanism. Model predictions are in reasonably good agreement with the observed salt-to-heat flux ratios.

We are using a flow-visualization technique, developed by Baker (Ref. 9), that employs thymol blue to mark fluid particles. The method involves placing the tracer, thymol blue, in the lower convective layer. Because thymol blue is a pH indicator, the color of the solution can be altered locally by the creation of ions at the surface of a grid electrode. This dyed fluid reveals the details of the flow.

The visualization experiments were performed in a bottom-heated plastic tank approximately 30 cm by 30 cm by 75-cm deep. The sides and bottom of the tank were insulated with about 7.5 cm of styrofoam. Sections of the side insulation were removed to permit us to make observations and to take pictures. A grid electrode was suspended about one cm below the gradient zone/lower convective zone interface. Temperature data and salinity data were obtained from a traversing rake containing a platinum resistance thermometer and a point conductivity probe.

Figure 2 shows the flow patterns immediately below the interface separating the nonconvecting region and the lower convecting region. Plumes of cold dyed fluid are clearly visible descending from the interface. Patterns of this type were observed repeatedly. A plume structure such as that in Fig. 2 agrees very well with the convective breakdown assumed in the mechanistic model.

Quantitative measurements using the dye have proved difficult. During observations made with heat fluxes in the range of 50 to 90 W/m^2, plume velocities ranged between 0.1 and 0.2 cm/s. The average plume velocity appeared to increase with increasing heat flux. Plume spacing ranged from 3 to 6 cm.

4. QUANTITATIVE TANK EXPERIMENT

4.1 Experiment and Data

We have begun a series of experiments designed to provide information on interface motion and on interface salt flux and heat flux in double diffusive flow.

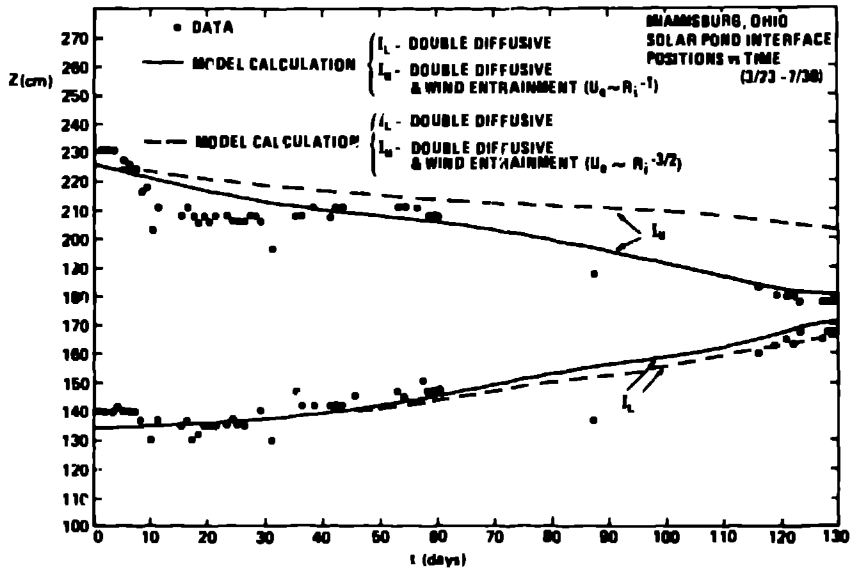

Fig. 1.
Comparison of measured and calculated interface positions for the Miamisburg, Ohio, salt-gradient solar pond.

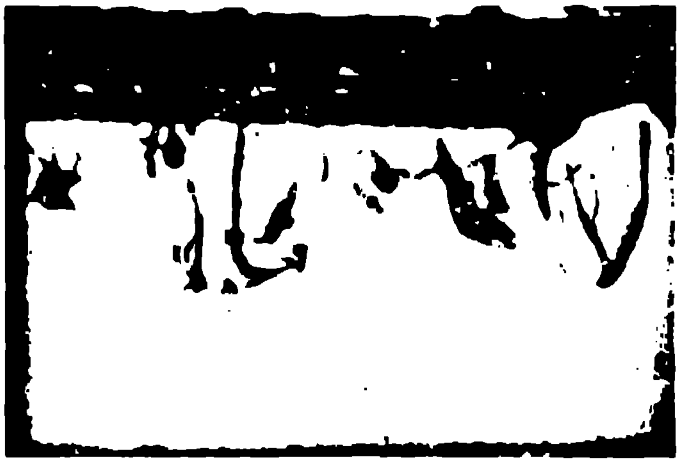

Fig. 2.
Thermal plumes observed about 1 cm below the gradient region/lower convective region interface during laboratory flow-visualization experiment.

The laboratory apparatus consists of a glass dewar (29-cm I.D. by 75-cm deep) with a bottom-heating element and a top-cooling plate to establish the desired temperature gradient. In order that we simulate a one-dimensional section of a solar pond, we were obliged to minimize radial heat loss. We accomplished this by using a guard heater that maintains the outside wall of the dewar at the same temperature as the fluid within.

Instrumentation for the tank consists primarily of a combined platinum resistance thermometer and a point conductivity probe mounted on a vertical traversing mechanism for detailed profile measurements in the neighborhood of the interfaces. A fixed vertical array of resistance thermometers provides overall temperature profiles. Solution samples taken from the lower convecting region provide calibration data for the salinity probe.

The results from our first experiment include information on the motion of the interface between the lower convective region and the gradient region as a function of time and the salt flux and heat flux across the interface.

Our measured salt-to-heat flux ratio was 0.30 ± 0.05 at a heat flux of 35.5 ± 2.0 W/m^2. This data point is plotted on Fig. 3, with the results of Marmorino and Caldwell (Ref. 7), Nielsen (Ref 10), and Broughton (Ref. 11). Figure 3 shows that our data point agrees reasonably well with the high range of data from Marmorino and Caldwell, but is higher than the Nielson and the Broughton results.

Our salt flux was obtained by comparing salinity profiles obtained at times t_1 and t_2. The interface position at time t_2 was obtained from salinity profiles

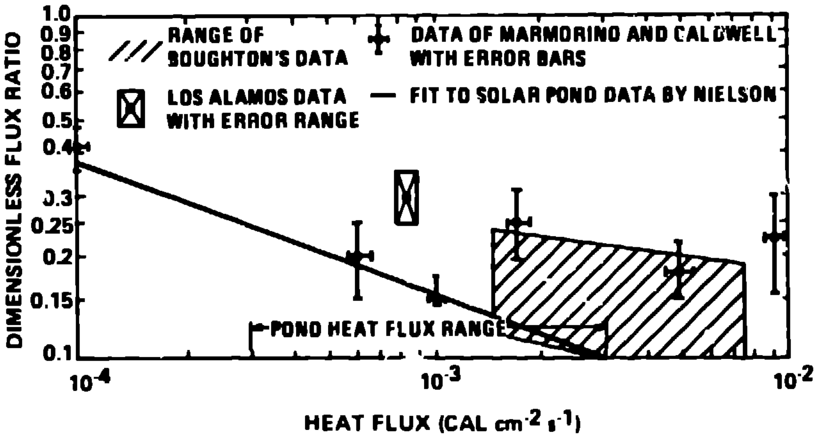

Fig. 3. Experimentally measured values of the dimensionless salt-to-heat flux ratio vs heat flux.

and temperature profiles; the salt content of the lower convecting layer was calculated from the height of the layer and its salinity as determined by specific gravity and temperature measurements. Salt was totaled at time t_1 for all the fluid below the t_2 interface position. The difference in salt content divided by time and by area produced the average salt flux between times t_1 and t_2. The heat flux was determined from the temperature gradient in the non-convecting region.

Our largest source of error was in determining the position of the interface. The salinity-profile data were scattered, whereas the temperature profiles were smooth and rounded in the region of the interface. We defined the interface as the intersection of the straight line extension of the gradient region temperature profile and the constant temperature line of the lower convecting region.

4.2 Model Calculation

Using the numerical model described in Section 2.1, we calculated the experiment described in Section 4.1. We used initial temperatures, salinity profiles, and heating rates based on the data. Calculations were performed with a number of salt-to-heat flux ratios. The lower interface position, lower convective region temperatures, and lower convective region salinity for a calculation with salt-to-heat flux ratio of 0.25 are compared with the experiment in Fig. 4. The agreement is reasonably good with the exception of the calculated interface growth rate for the first two days. This may be caused by our use of approximate initial profiles in the calculation. A flux ratio of 0.25 is at the low end of the experimental range; calculations performed with higher flux ratios produced a growth rate of the lower region that was too rapid, whereas lower flux ratios gave a somewhat lower growth rate than that observed.

With additional research, we hope to produce more precise results for validation of the numerical model.

5. NOMENCLATURE

- C_D Drag coefficient
- C_p Specific heat (J/g°C)
- d Depth of upper convecting layer (cm)
- D_s Salt diffusivity (cm^2/s)
- D_{ST} Soret coefficient (g/cm s°C)
- D_T Thermal diffusivity (cm^2/s)
- $\hat{D}_s$ Effective boundary layer diffusivity (cm^2/s)
- F_s Salt flux (g/cm^2 s)
- g Gravitational acceleration (cm/s^2)
- H Heat flux (W/cm^2)
- k_T Thermal conductivity (W/cm°C)
- $\hat{k}_T$ Effective boundary layer conductivity (W/cm°C)
- L Energy removed at depth x (W/cm^3)
- q Solar energy absorbed at depth x (W/cm^3)
- Ri Richardson number,

$$Ri = \frac{g}{\rho} \frac{\partial \rho}{\partial x} \frac{d^2}{u_*^2}$$

- T Temperature (°C)
- u_e Entrainment velocity (cm/s)
- u_* Friction velocity (cm/s)
- w Wind speed (cm/s)
- x Vertical distance (cm)
- α Thermal coefficient of expansion (1/°C)
- β Salinity expansion coefficient (cm^3/g)
- ρ Fluid density (g/cm^3)
- ρ_a Air density (g/cm^3)
- ρ_s Solute density (g/cm^3)

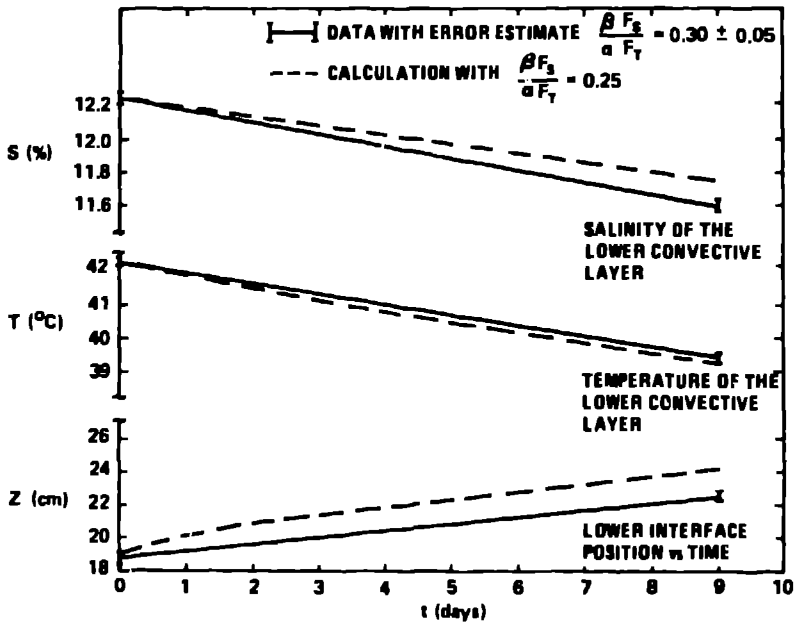

Fig. 4.
Comparison of observed and calculated salinity, temperature, and interface position vs time for laboratory-tank experiment.

6. ACKNOWLEDGEMENTS

The authors would like to thank K. Hedstrom and C. Bates for their contributions to the flow-visualization work and to J. Hauser, J. Tafcya, B. Ketchum, L. Dalton, and F. Lujan for their assistance with the experimental apparatus and instrumentation.

7. REFERENCES

1. K. A. Meyer, "A One-Dimensional Model of the Dynamic Layer Behavior in a Salt Gradient Solar Pond," in Proc. of the International Solar Energy Society Meeting, Philadelphia, Pennsylvania, May 26-30, 1981 (American Section of the International Solar Energy Society, Newark, Delaware, 1981), p. 763.

2. G. O. Marmorino and D. R. Caldwell, "Heat and Salt Transport Through a Diffusive Thermohaline Interface," Deep Sea Research, 23, 59 (1976).

3. P. F. Crapper, "Fluxes of Heat and Salt Across a Diffusive Interface in the Presence of Grid-Generated Turbulence," Int. Jour. Heat and Mass Transfer, 19, 1371 (1976).

4. J. S. Turner, "The Influence of Molecular Diffusivity on Turbulent Entrainment Across a Density Interface," Journal of Fluid Mechanics, 33, 639 (1968).

5. J. Wu, "Wind-Induced Turbulent Entrainment Across a Stable Density Interface," Journal of Fluid Mechanics, 61, 275 (1973).

6. E. Kit, E. Berent, and M. Vajda, "Vertical Mixing Induced by Wind and Rotating Screen in a Stratified Fluid in a Channel," Journal of Hydraulic Research, 18, 35 (1980).

7. W. R. Lindberg and R. D. Haberstroh, "A Thermohaline Convection Model," Office of Naval Research Project NR-083-250, Tech. Report No. 1, November 1971.

8. P. F. Linden and T. G. L. Shirtcliffe, "The Diffusive Interface in Double Diffusive Convection," Journal of Fluid Mechanics, 87, 417 (1978).

9. D. J. Baker, " A Technique for the Precise Measurement of Small Fluid Velocities," Journal of Fluid Mechanics, 26, 573 (1966).

10. C. E. Nielson, "Control of Gradient Zone Boundaries," in Proc. of the International Solar Energy Society Meeting, Atlanta, Georgia, May 28, 1979 (American Section of the International Solar Energy Society, Newark, Delaware, 1981), p. 1010.

11. J. M. Broughton, "Experiments on Steady Layered Convection in a Doubly Diffusive System," Masters Thesis, Colorado State University, Dept. of Mechanical Engineering (1977).